*Acta of Bioengineering and Biomechanics*
*Vol. 13, No. 2, 2011*

Original paper

# Strain-rate sensitivity of porcine and ovine corneas

AHMED ELSHEIKH[1]*, WAEL KASSEM[2], STEPHEN W. JONES[1]

[1] School of Engineering, University of Liverpool, UK.
[2] Division of Civil Engineering, University of El-Minia, El-Minia, Egypt.

Knowledge of strain-rate sensitivity of corneal tissue is important for improving the understanding of the tissue's response to mechanical actions and the accurate numerical simulation of corneal biomechanical behaviour under the effects of disease and surgery. In the study, fresh and well-preserved porcine and ovine corneal buttons were subjected to uniaxial tension loads with seven different strain rates ranging between 0.8 and 420% per minute. All specimens exhibited increased stiffness (as measured by the tangent modulus) with higher strain rates. However, clear differences in their behaviour were observed. While ovine corneas showed gradual, consistent and mostly statistically significant increases in stiffness with all elevations in strain rate, porcine corneas' response was significant over only a limited range of low strain rates. The effect of strain rate on the material's stress-strain behaviour was considered in the formation of three sets of constitutive models including: (i) a model based on a simple exponential stress–strain relationship, (ii) the Ogden model that considers the tissue's hyperelasticity but not anisotropy, and (iii) a third model by Holzapfel, Gasser and Ogden that considers both hyperelasticity and anisotropy. The three models are introduced to enable consideration of the strain rate effects in simulations employing finite element programs with varying capabilities or in modelling applications in corneal biomechanics which may or may not require consideration of mechanical anisotropy.

*Key words*: *cornea, mechanical behaviour, strain-rate effects, experimental testing*

## 1. Introduction

The cornea is a load-bearing tissue whose primary function is to focus light on the retina. The mechanical properties of the cornea are important in maintaining this function under the effect of actions such as intraocular pressure (IOP), eyelid movement and external impacts. Significant advances have been made in understanding the cornea's instantaneous response to mechanical actions [1]–[3] and the long-term stress–relaxation and creep behaviour [4], [5]. Little progress, however, has been made in quantifying the cornea's dependence on strain rate that, in line with most other biological tissues, can make the cornea stiffer under higher strain rates.

Recent experimental studies confirmed the cornea's nonlinear behaviour under loading, with increasing tangent modulus (measure of mechanical stiffness) under higher stresses [1], [6], [7]. The studies used both animal and human tissue tested under either uniaxial tension or inflation conditions, and resulted in constitutive models, or stress–strain relationships, in forms suitable for use in numerical simulations of ocular behaviour [4], [8]. However, in most of the studies, their experimental tests were conducted under a particular load or strain rate, and although the potential effects of strain-rate dependence were mentioned, they were not quantified. This makes the material's constitutive models suitable only for the strain-rates under which they were developed, and knowledge is currently unavailable on how to consider the effect of changing the strain rate on the material's behaviour.

This study is intended to address this need through an experimental assessment of the strain-rate depend-

* Corresponding author: Ahmed Elsheikh, School of Engineering, University of Liverpool, Liverpool L69 3GH, UK. Tel: 0044 151 7944833, e-mail: ahmed.elsheikh@liv.ac.uk

Received: March 2nd, 2011
Accepted for publication: May 16th, 2011

ence of corneal tissue. In preparation for work on human corneas, the study starts with porcine (pig) and ovine (sheep) tissues because of their wide availability and as they offer a degree of mechanical and microstructural similarity to human corneas [4], [9], [10]. Porcine, ovine and human corneas have been reported to have similar interfibrillar Bragg spacing (58.6, 60.4 and 55.3 nm), fibril diameter (36.9, 37.0 and 30.8 nm), intermolecular Bragg spacing (1.57, 1.59 and 1.63 nm) and number of molecules per fibril cross-section (378, 380 and 263) [11]. Therefore, although the behaviour of human corneas is expected to be somewhat different from that reported in this study, the behaviour trends and the techniques used are likely to be similar.

Further, the strain-rate dependence of porcine and ovine corneal tissue, as determined experimentally, has been considered in the development of constitutive models that describe tissue behaviour in numerical simulations. Three constitutive model types that consider material hyper-elasticity and anisotropy have been adopted in this part of the study.

## 2. Materials and methods

Eight porcine and eight ovine eyes from animals aged between 4 and 6 months were obtained fresh from a local abattoir and prepared for tests within 6–9 hours post-mortem. Only one eye per animal was used in the study. The vertical (superior–inferior) anatomical direction was identified using the location of the optic nerve and the clear difference between the cornea's vertical and horizontal diameters. A corneal button with 3–4 mm scleral ring was extracted from each eye using a pair of curved scissors, and the iris, lens and ciliary body were removed. Following extraction, corneas were placed in preservation medium Eusol-C

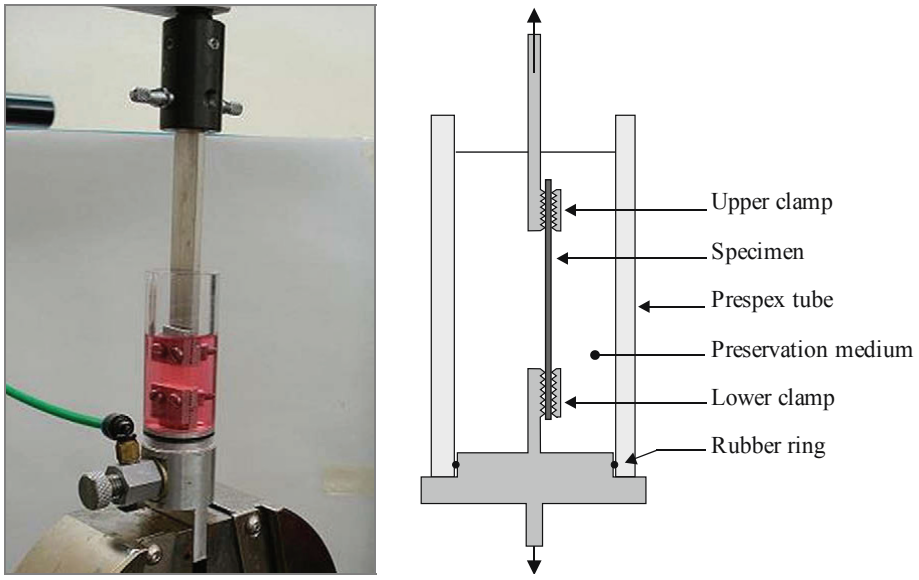


Fig. 1. Test setup showing a specimen connected to two end clamps while being preserved in Eusol-C

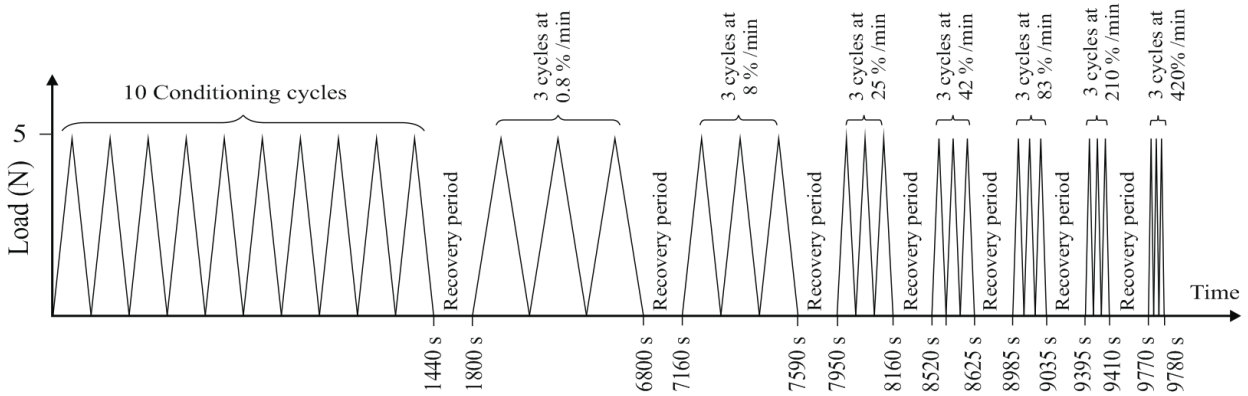


Fig. 2. Strain-controlled loading regime

(Alchima, Padova, Italy), then taken out and prepared for testing one by one. The specimens were not frozen at any stage.

A strip specimen with 4.4 mm width was obtained from the central region of each cornea in the vertical direction using a double-blade tool. The specimens were connected to mechanical clamps with rough surfaces to prevent slippage, see figure 1. The clamps held the 3 mm long end strips of scleral tissue in addition to about 1–2-mm length of corneal tissue in the limbal region, leaving about 12 mm of corneal tissue between clamp edges. The thickness of each specimen was measured using an ultrasound pachymeter (Pachmate 55, DGH Technologies, Exton, Pa). Three measurements were performed at the cornea strip's centre and close to the clamps, and the results used in later analysis. The average and standard deviations of thickness values were 971.5 ± 75.7 μm and 1013.1 ± 67.8 μm at the centre and edge of porcine corneas, respectively, and 828.6 ± 127.5 μm and 882.3 ± 87.2 μm for ovine corneas.

Before the start of a test, a perspex tube was placed around the specimen and filled with Eusol-C to maintain stromal hydration during the tests. Once testing was complete, Eusol-C was drained and the specimen removed for visual inspection. Testing was performed at room temperature, 21 °C, on an Instron 3366 materials testing machine (Instron, Norwood, MA) equipped with a 10 N capacity load cell.

Specimens were subjected to an initial set of ten cycles of loading and unloading between 0 and 5 N (which was sufficient to go beyond the hyperelastic behaviour stage in all tests) with a low strain rate of 8% per minute to condition the tissue, stabilise its mechanical behaviour and ensure a reproducible response to uniaxial testing, figure 2. This was followed by seven sets of three load cycles with different strain rates: 0.8, 8, 25, 42, 83, 210 and 420% per minute ($\text{min}^{-1}$). Each of the seven sets included two initial cycles to condition the tissue at a particular strain rate before considering the results in a third cycle as representative of the cornea's biomechanical behaviour under that rate. Between each two sets of cycles, the specimens were allowed to recover their initial length to reduce the dependence of the behaviour on the strain history of preconditioning cycles [12]. This process took between 4 and 7 minutes in all cases. The maximum stress adopted (1.2–1.35 MPa), although higher than would be expected under normal intraocular pressure values, was selected to ensure coverage of the whole nonlinear stage of corneal behaviour.

The lowest strain rate considered was close to that experienced under an intraocular pressure (IOP) change from standing or seated to supine position – reported to be about 6 mm Hg taking place in a few seconds [13], while the highest rate was above that expected under abnormal eye rubbing [14], but lower than those associated with impacts or non-contact tonometry [15].

The test output comprised the axial tension load $T$ in Newtons and the specimen elongation $\delta$ in mm. These values were stored every 0.1 sec for later analysis. $T$ and $\delta$ were converted into values of stress $\sigma$ and strain $\varepsilon$, following a mathematical process explained earlier [8], [16], which took into account the variable specimen thickness.

## 2.1. Constitutive models

Constitutive models have been used to demonstrate the effect of strain rate on the material's stress–strain behaviour as obtained experimentally. In order to enable application of different methods to numerical simulation, three types of constitutive model have been adopted, the first of which is based on a simple exponential relationship between stress and strain that has been found suitable in earlier studies [17]:

$$\sigma = a\,(e^{b\,\varepsilon} - 1)\,, \tag{1}$$

where $a$ and $b$ are constants. This form enables the quick generation of stress–strain behaviour, which can be input directly into a number of finite element (FE) packages or further manipulated to generate other stress–strain relationship forms such as those included below.

The second type of the constitutive model adopted is the strain energy function developed by Ogden, which has been widely used to describe the nonlinear hyperelastic behaviour of biological materials [18], [19]. This model, which is primarily suitable for isotropic materials, is adopted here as a useful approximation since the more appropriate anisotropic strain energy functions (one of which is considered below) are not yet available in several commercial FE packages, which are commonly used in the predictive analysis of nonlinear corneal behaviour. According to Ogden's function, the strain energy density per unit volume $W$ is calculated as:

$$W = \sum_{i=1}^{N} \frac{2\,\mu_i}{\alpha_i^2} (\overline{\lambda}_x^{\alpha_i} + \overline{\lambda}_y^{\alpha_i} + \overline{\lambda}_z^{\alpha_i} - 3) + \sum_{i=1}^{N} \frac{1}{D_i} (J-1)^2, \tag{2}$$

where $\overline{\lambda}_k$ are the deviatoric principal stretches = $J^{-1/3} \times \lambda_k$ ($k = x, y, z$); $\lambda_x$, $\lambda_y$, $\lambda_z$ the principal stretches in the three main Cartesian directions along specimen

width, thickness and length, respectively; $J = \lambda_x.\lambda_y.\lambda_z$; $\alpha_i$ and $\mu_i$ ($i$ = 1 ... $N$) are material parameters denoting the strain hardening exponent and the shear modulus, respectively; and $N$ is the function order. As corneal tissue can be approximated as an almost incompressible material [20], [21], the product of stretch in all three directions, $J = \lambda_x.\lambda_y.\lambda_z = 1$, therefore the second term of equation (2) can be omitted, and the equation can be written in terms of stress as:

$$\sigma_z = \sum_{i=1}^{N} \frac{2\,\mu_i}{\alpha_i} \left(\lambda_z^{\alpha_i - 1} - \lambda_z^{-1-\alpha_i/2}\right). \tag{3}$$

The values of material parameters $\alpha_i$ and $\mu_i$ can be determined by fitting the function to the experimental stress–strain results through an error minimisation process:

$$\Sigma\, abs(\sigma_{\text{equation}} - \sigma_{\text{experiment}}) = \text{minimum}.$$

As described in section 3, the fit with a first-order equation was not satisfactory in most cases, and a second order ($N$ = 2) or a third order ($N$ = 3) would be recommended.

Finally, the micro-structural and mechanical anisotropy of the cornea [8], [22] could be considered by a development of the hyperelastic constitutive model described above, in which anisotropy has been introduced. This has been done by considering the strain energy function proposed by Holzapfel, Gasser and Ogden [23], [24]:

$$W = C_{10}\,(\bar{I}_1 - 3) + \frac{1}{D}\left(\frac{J^2 - 1}{2} - \ln J\right) + \frac{k_1}{k_2}\sum_{\alpha=1}^{Nf} \left(e^{k_2\,\bar{E}_\alpha^{\,2}} - 1\right), \tag{4}$$

where $C_{10}$, $D$, $k_1$, $k_2$, and $\bar{E}_\alpha$ are material parameters; $Nf$ is the number of the families of fibres ($Nf \leq 3$); $\bar{I}_1$ the first invariant of the deviatoric part of the left Cauchy–Green deformation tensor; $\bar{I}_1 = J^{-2/3} \times I_1$, and $I_1 = \lambda_1^2 + \lambda_2^2 + \lambda_3^2$, where $\lambda_i$ are the principal stretches. The first two terms in equation (4) represent the distortional and volumetric contributions of the non-collagenous isotropic extracellular matrix of the stroma, and the third term represents the contributions from the different families of collagen fibres. With corneal tissue considered to be incompressible, $J$ = 1, and as a result the second term can be omitted. Another basic assumption of the model is that collagen fibres can support tension only and would buckle under compressive loading. Therefore, the anisotropic contribution in the strain energy function appears only when the strain of the fibres is positive.

$\bar{E}_\alpha$ is a Green–Lagrange strain-like quantity which characterises for each family of fibres the strain in the direction of the mean orientation of the fibres. $\bar{E}_\alpha$ is replaced by

$$\kappa\,(\bar{I}_1 - 3) + (1 - 3\kappa)\,(\bar{I}_4 - 1),$$

where $\bar{I}_4$ is a tensor invariant equal to the square of the stretch ($\lambda^2$) in the mean direction of the fibre family. The parameter $\kappa$ describes the level of dispersion in the fibre directions and is given by the formula:

$$\kappa = \frac{1}{4}\int_0^{\pi} \rho(\theta)\,\sin^3\theta\; d\theta\,,$$

where $\rho(\theta)$ is the distribution function that characterises the orientation density of the fibres in terms of radial angle $\theta$ with respect to the main direction.

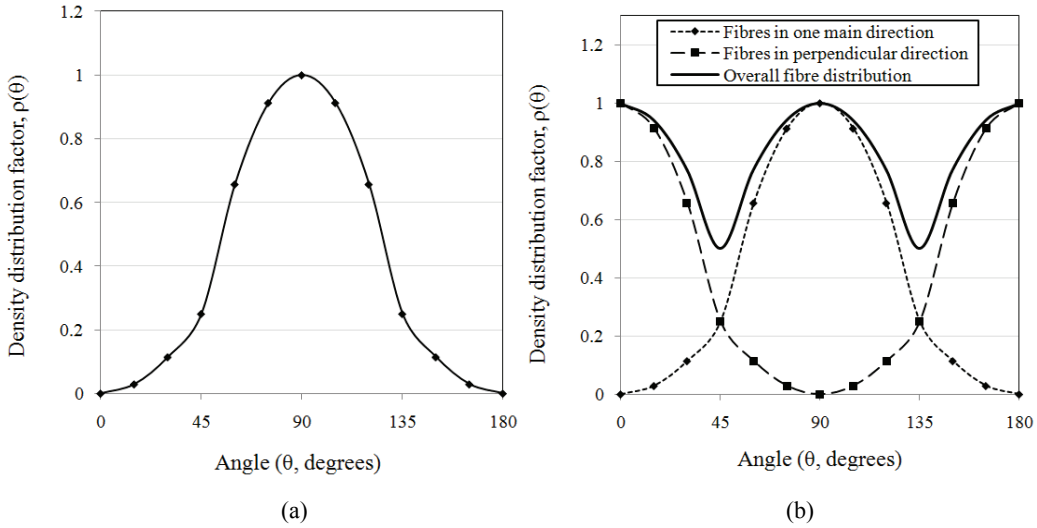


(a) (b)

Fig. 3. The angular distribution function of one family of fibres (a), and both families of fibres along with the combined distribution of the two families (b)

The model assumes that there are two families of collagen fibres ($Nf = 2$) with mean preferred vertical and horizontal directions, respectively. Within each family, the fibres are dispersed with rotational symmetry about the mean direction. Earlier microstructural studies [22], [25], [26] indicated that 2/3 of all stromal collagen fibres are positioned in, and shared equally between, the 45° sectors surrounding the vertical and horizontal directions, with the remaining 1/3 shared equally between the 45° sectors surrounding the 45° and 135° directions. Splitting the fibres into two families means that for each family 1/3 of all fibres are oriented between ± 22.5° around the main direction, and 1/12 within each of the adjacent 45° sectors. This distribution was smoothed and approximated using the following distribution function (figure 3):

$$\rho(\theta) = \begin{cases} \dfrac{\sqrt{2}}{4}\dfrac{1-\cos\theta}{\sqrt{2}-1} & \text{for } \theta = 0 \text{ to } \dfrac{\pi}{4} \\ \dfrac{\sqrt{2}\,(3\sin\theta+1)-4}{4\,(\sqrt{2}-1)} & \text{for } \theta = \dfrac{\pi}{4} \text{ to } \dfrac{3\pi}{4} \\ \dfrac{\sqrt{2}}{4}\dfrac{1-\cos\theta}{\sqrt{2}-1} & \text{for } \theta = \dfrac{3\pi}{4} \text{ to } \pi \end{cases}. \quad (5)$$

Using this distribution function, the value of $\kappa$ is obtained from

$$\kappa = \frac{1}{4}\int_0^{\pi} \rho(\theta)\,\sin^3\theta\; d\theta$$

as 0.242, which is within the limits of 0 (perfect alignment) $\leq \kappa \leq$ 0.33 (random distribution). This leaves only three material parameters ($C_{10}$, $k_1$ and $k_2$) to be determined for each set of tests from fitting equation (4) to the average experimental results of the set while minimising the error $\Sigma\, abs(\sigma_{\text{equation}} - \sigma_{\text{experiment}})$.

## 2.2. Statistical analysis

The tests of statistical differences for comparisons between specimen groups were performed with the Chi-square test. The significance of associations between strain rate and mechanical stiffness (as measured by the tangent modulus) was assessed by Spearman rank correlation. Analyses were performed in SPSS 17.0 (SPSS Inc., Illinois). $P < 0.05$ was considered an indication of statistical significance.

# 3. Results

## 3.1. Experimental behaviour

An example set of results for a porcine specimen is shown in figure 4 including the load–elongation behaviour under different strain rates, the corresponding stress–strain behaviour and the variation of the tangent modulus $E$ (measure of material stiffness) with stress. Specimens exhibited nonlinear load–elongation and stress–strain behaviour with an initial low tangent modulus increasing gradually under higher stresses. The transition from low to high stiffness was gradual as can be seen in figure 4b, although it was faster at

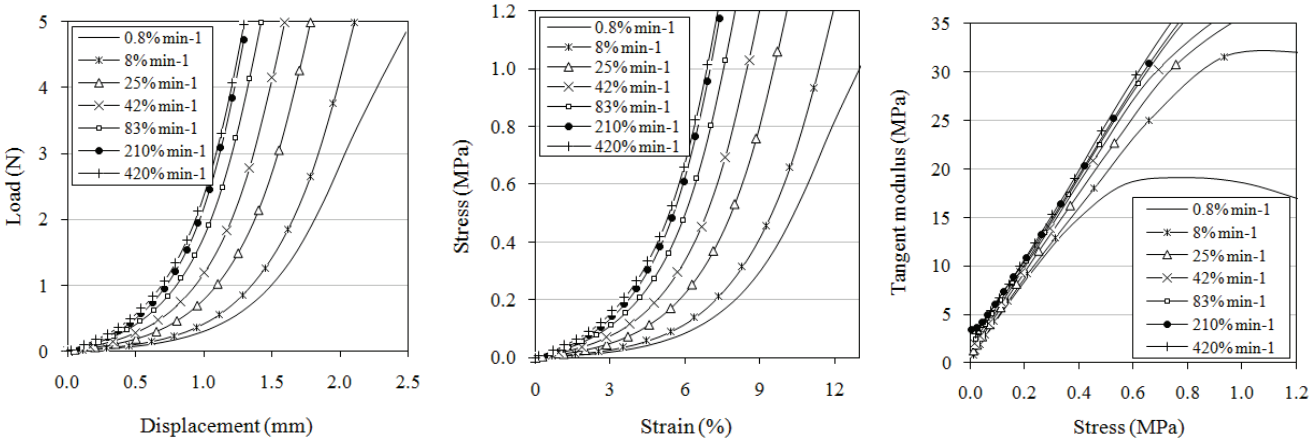


Fig. 4. Example results of a porcine cornea including the load–elongation behaviour under different strain rates (a), the corresponding stress–strain behaviour (b), and the tangent modulus–stress behaviour (c)

low stress levels. This form of behaviour persisted regardless of the strain rate employed and was valid for both porcine and ovine corneas.

Converting the stress–strain results to $E$–$\sigma$ behaviour, as in figure 4c, showed a linear relationship covering most of the test stress range. This could be related to the fact that the stress–strain results fitted closely an exponential relationship of the form: $\sigma = a(e^{b\varepsilon} - 1)$, which when differentiated produced a linear $E$–$\sigma$ behaviour:

$$E = d\sigma / d\varepsilon = a\, b\, .\, e^{b.\varepsilon} = b\, .\, (\sigma + a).$$

Figure 5 further shows example results of the variation of material stiffness (as measured by the tangent modulus $E$) with the progression of load cycles. After considerable stiffening in the first (and sometimes the second) cycle, the $E$–$\sigma$ behaviour appeared to have stabilised. Subsequent changes in the strain rate required further conditioning but the corresponding changes in $E$ were limited to below 5%. This finding justified using the results of the last cycle within each test stage as representative of the specimens' stable behaviour. Although the results shown in figures 4 and 5 were for a porcine cornea, they were typical of most specimens tested, including those obtained from ovine corneas.

## 3.2. Strain-rate effects

The average stress–strain behaviour of porcine and ovine corneas is shown in figure 6. In both cases, there was gradual stiffening with increases in strain rate. The results show a large and statistically significant ($P < 0.05$) increase in stress with increasing the strain rate from 0.8% min$^{-1}$ to 25% min$^{-1}$ in porcine corneas. Further increases in stress followed with

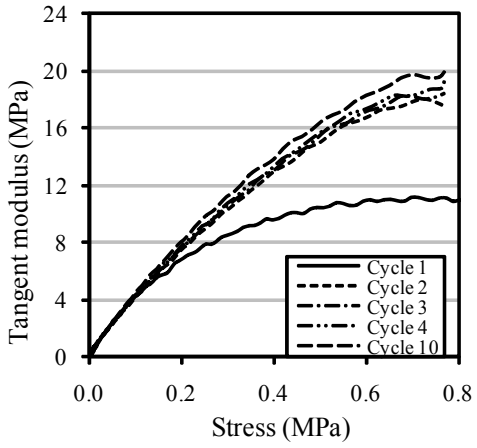


a)

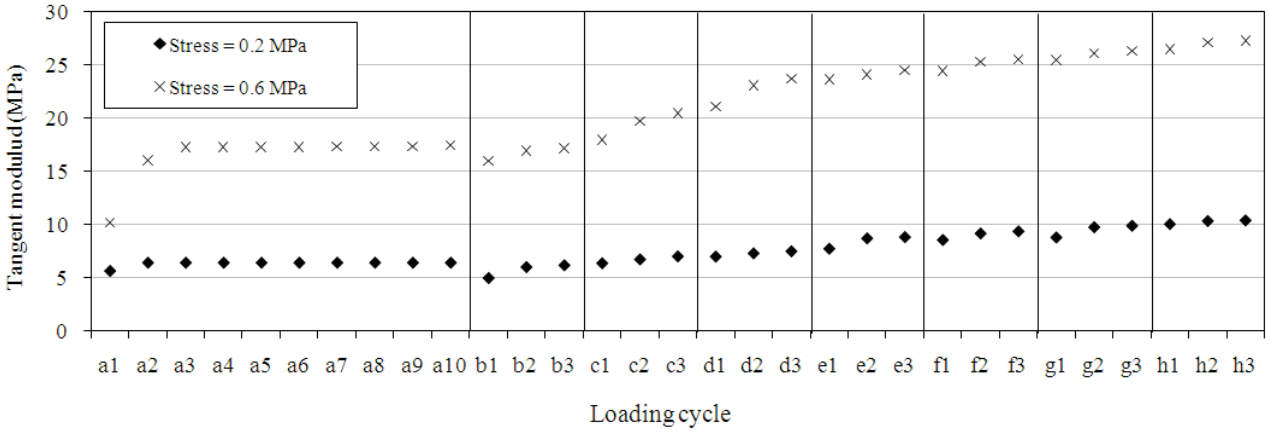


(b)

Fig. 5. A typical example results of the effect of conditioning in stabilising the mechanical behaviour of a porcine cornea. The results show the variation of $E$-stress behaviour over the first 10 cycles of loading (since the behaviour change between cycles 4 and 10 was negligible, results for cycles 5 to 9 were omitted for clarity) (a), and the variation of $E$ at different stress levels with the progression of load cycles (b)

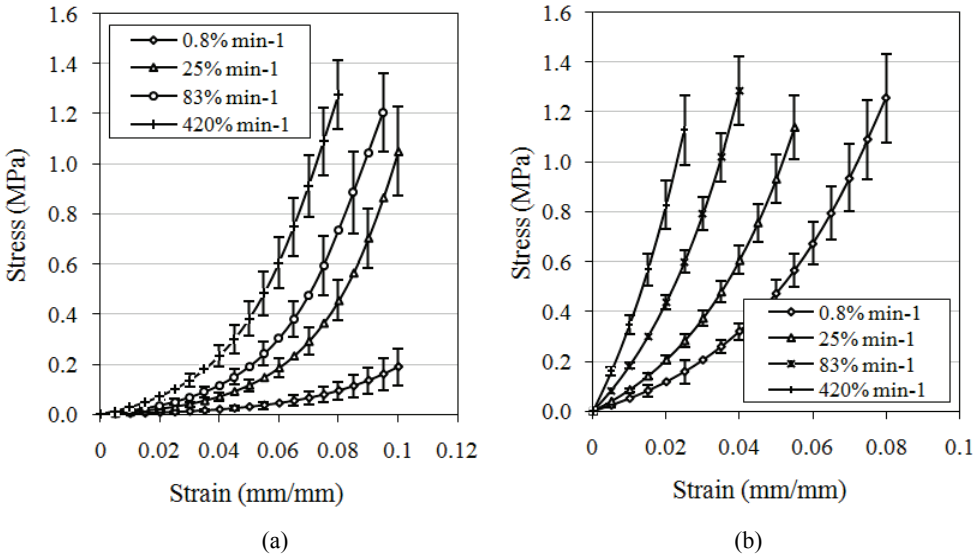


Fig. 6. Average behaviour of porcine (a) and ovine (b) corneas at different strain rates. Only the behaviour associated with 4 strain rates is shown for clarity

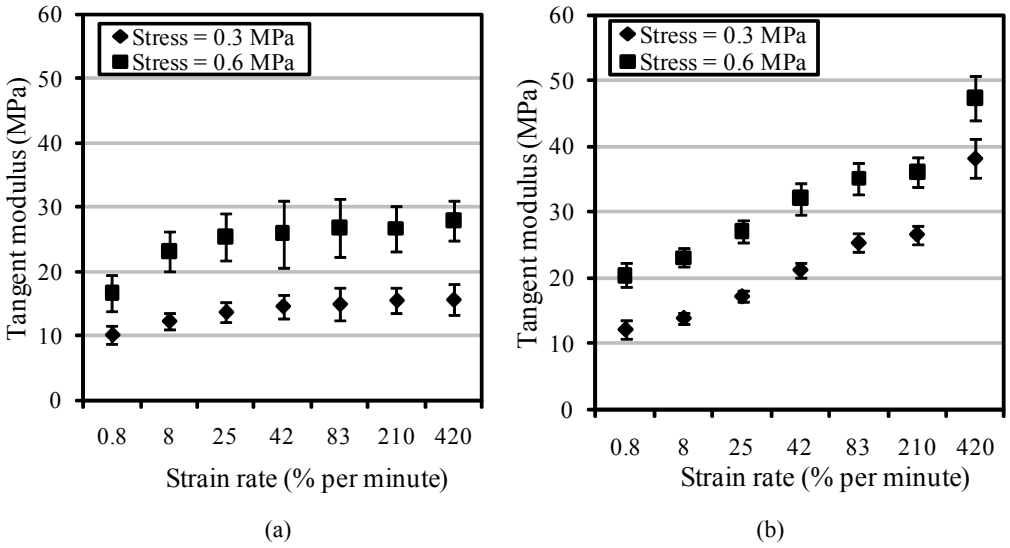


Fig. 7. Effect of strain rate on the values of tangent modulus of porcine corneas (a), and ovine corneas (b) at two intermediate stress levels of 0.3 and 0.6 MPa

higher strain rates, but the stepped changes were statistically insignificant. On the other hand, ovine corneas continued to demonstrate statistically significant ($P < 0.05$) increases in stress with most changes in strain rate.

Figure 7 presents the average and standard deviation of the tangent modulus at two intermediate stress levels over the seven strain rates considered. The figure shows that porcine corneas experienced large (40.2% on average) and statistically significant ($P < 0.05$) increases in $E$ with changes in strain rate from 0.8 to 8% min$^{-1}$. Subsequent increases in strain rate led to much lower, and statistically insignificant, increases in $E$. On average, $E$ at 420% min$^{-1}$ strain rate was only 26.1% higher than that in the tests conducted at 8% min$^{-1}$, and the difference in $E$ results between the two groups was not statistically significant ($P = 0.46$). Ovine corneas demonstrated markedly different behaviour with gradual and mostly statistically significant increases in $E$ between each two consecutive strain rates. Compared to $E$ at 0.8% min$^{-1}$, $E$ at the faster strain rates were higher by 15.4 ± 11.1%, 40.8 ± 16.9%, 71.1 ± 21.2%, 100.6 ± 33.0%, 109.7 ± 36.9% and 208.7 ± 63.8%, respectively.

The stiffening of porcine and ovine corneas under higher stresses and their response to variations in strain

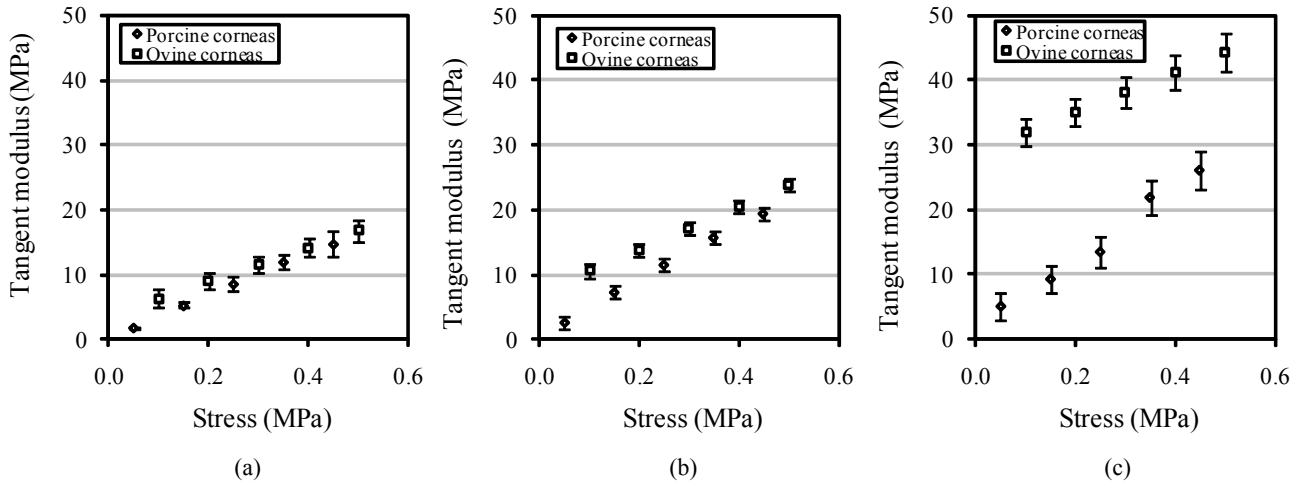


Fig. 8. Tangent modulus values of porcine and ovine corneas at 0.8% $min^{-1}$ strain rate (a), 25% $min^{-1}$ rate (b) and 420% $min^{-1}$ rate (c)

rate are compared in figure 8. The figure presents comparisons of $E$ values of porcine and ovine corneas at different stress levels and three strain rates, including the lowest (0.8% $min^{-1}$), the highest (420% $min^{-1}$) and an intermediate value (25% $min^{-1}$). In all cases, $E$ increased with stress, as would be expected with the material's collagenous content. However, it is evident that the difference between the $E$ values for porcine and ovine corneas changed considerably – was small at 0.8% $min^{-1}$ (32% on average – range = 14–69%) and increased gradually to 42% (20–49%) with 25% $min^{-1}$ and 133% (46–176%) under 420% $min^{-1}$ rate. The large difference under 420% $min^{-1}$ strain rate reflects the difference in behaviour between porcine and ovine corneas, where the former experienced stable behaviour with strain rates above 8% $min^{-1}$ while the latter continued to undergo large increases in $E$ with all additions to the strain rate (figure 7).

## 3.3. Strain-rate material parameters

For most of the behaviour observed, both porcine and ovine corneas closely followed an exponential stress–strain relationship of the form $\sigma = a(e^{b\varepsilon} - 1)$, where $a$ and $b$ were constants. Beyond a certain high stress, the $\sigma$–$\varepsilon$ relationship became almost linear; $\sigma = c.\varepsilon + d$, with $c$ and $d$ being two more constants. Figure 9 presents a schematic description of the physical meaning of parameters $a$–$d$ and the two stages of hyperelastic and elastic material behaviour.

Fitting the two equation forms to each average stress–strain behaviour, and finding the stress level that separated the exponential and linear behaviour stages, and the values of constants $a$–$d$ were conducted while minimising the sum of absolute errors; $\Sigma\, abs(\sigma_{equation} - \sigma_{experiment})$. The values of the constants

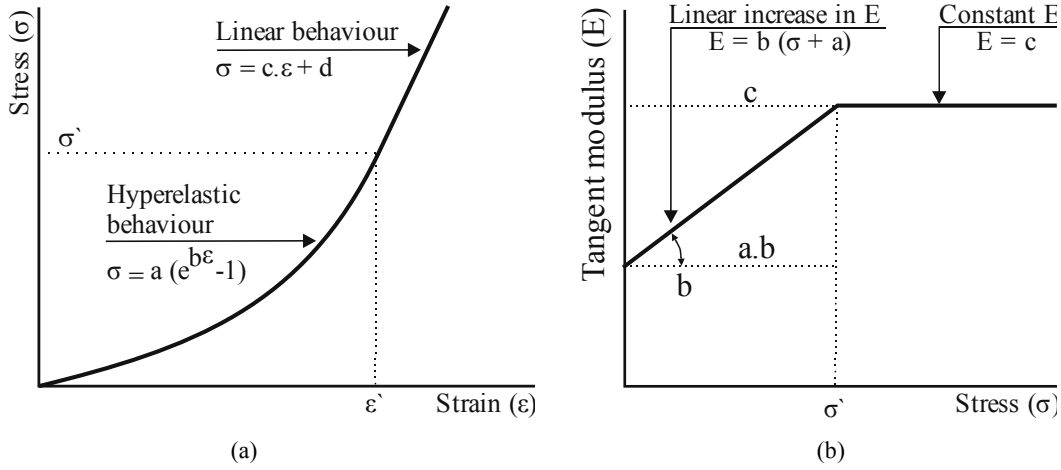


Fig. 9. Typical behaviour of corneal tissue including stress–strain behaviour (a), and tangent modulus–stress relationship (b)

Table 1. Values of equation parameters $a$, $b$, $c$ and $d$ that provide the best fit within each group of tests, and the stress $\sigma$ separating the exponential and linear behaviour stages

| Strain rate | Porcine specimens | | | | | Ovine specimens | | | | |
|---|---|---|---|---|---|---|---|---|---|---|
| | $a$ | $b$ | $c$ | $d$ | $\sigma$ | $a$ | $b$ | $c$ | $d$ | $\sigma$ |
| 0.8% min$^{-1}$ | 0.01 | 34.12 | 5.80 | –0.39 | 0.36 | 0.15 | 27.12 | 31.24 | –1.38 | 1.21 |
| 8% min$^{-1}$ | 0.01 | 39.54 | 18.55 | –1.39 | 0.46 | 0.15 | 30.55 | 48.07 | –1.54 | 1.42 |
| 25% min$^{-1}$ | 0.01 | 40.47 | 23.67 | –1.53 | 0.57 | 0.22 | 32.88 | 50.74 | –1.67 | 1.32 |
| 42% min$^{-1}$ | 0.02 | 41.40 | 28.78 | –1.67 | 0.67 | 0.29 | 35.46 | 57.29 | –1.64 | 1.32 |
| 83% min$^{-1}$ | 0.03 | 41.67 | 31.41 | –1.78 | 0.73 | 0.36 | 36.00 | 73.86 | –1.88 | 1.39 |
| 210% min$^{-1}$ | 0.05 | 41.72 | 38.86 | –1.79 | 0.85 | 0.38 | 39.00 | 72.50 | –1.47 | 1.48 |
| 420% min$^{-1}$ | 0.05 | 41.90 | 38.75 | –1.82 | 0.87 | 0.54 | 43.97 | 78.94 | –1.90 | 1.45 |

Table 2. Parameters of third-order Ogden's strain energy function (equation (3)) that provided the best fit with the experimental results

| Strain rate | Porcine specimens | | | | | | Ovine specimens | | | | | |
|---|---|---|---|---|---|---|---|---|---|---|---|---|
| | $\mu_1$ | $\alpha_1$ | $\mu_2$ | $\alpha_2$ | $\mu_3$ | $\alpha_3$ | $\mu_1$ | $\alpha_1$ | $\mu_2$ | $\alpha_2$ | $\mu_3$ | $\alpha_3$ |
| 0.8% min$^{-1}$ | –2.36 | 43.28 | 2.48 | 43.08 | –0.04 | 43.98 | –2.21 | 48.97 | 3.95 | 43.80 | –0.54 | –43.62 |
| 8% min$^{-1}$ | –2.34 | 43.10 | 2.49 | 43.26 | –0.02 | 43.98 | –2.61 | 53.97 | 4.60 | 48.71 | –0.57 | –45.61 |
| 25% min$^{-1}$ | –2.21 | 43.05 | 2.61 | 43.29 | –0.22 | 43.98 | –4.33 | 54.47 | 7.62 | 48.71 | –0.57 | –45.61 |
| 42% min$^{-1}$ | –2.44 | 50.96 | 3.27 | 48.73 | –0.91 | 41.19 | –6.04 | 54.47 | 10.79 | 48.71 | –0.57 | –104.32 |
| 83% min$^{-1}$ | –2.54 | 52.94 | 3.49 | 50.30 | –1.00 | 40.78 | –8.25 | 54.47 | 14.51 | 48.71 | –0.57 | –104.32 |
| 210% min$^{-1}$ | –2.83 | 55.52 | 4.36 | 51.46 | –1.43 | 40.31 | –8.26 | 54.73 | 14.84 | 48.71 | –0.57 | –104.32 |
| 420% min$^{-1}$ | –2.86 | 55.69 | 4.54 | 51.28 | –1.31 | 40.31 | –12.15 | 54.73 | 21.22 | 48.71 | –0.57 | –104.32 |

for tests with different strain rates on porcine and ovine corneas are listed in table 1. With these values, the average error: $\Sigma\, abs(\sigma_{equation} - \sigma_{experiment})$ per each behaviour point remained below 0.01 MPa. The table shows gradual increases in the values of $a$ and $b$ indicating both higher initial $E$ values (= $a.b$) and faster increases in $E$ with stress (dependent on $b$) with higher strain rates. There was also a gradual increase in $c$ with strain rate, meaning higher $E$ values within the final linear stage of a specimen's stress–strain behaviour.

The effect of varying the strain rate on the values of $\alpha$ and $\mu$ parameters of the Ogden strain energy function (equation (3)) is illustrated in table 2. The results include those obtained from fitting the average experimental results of each strain rate to the Ogden function of the third order ($N = 3$). The average absolute errors ($\Sigma\, abs(\sigma_{predicted} - \sigma_{experimental}) / n$, where $n$ is the number of data points) reduced significantly with increasing the function order, as illustrated in table 3. In most cases, the improvement of the quality of fit continued with increasing the function order, and it was necessary to adopt $N = 3$ to achieve a close match with the experimental results. However, attempting $N = 4$ produced little further improvement in accuracy. An example of the close fit with the experimental results achieved with $N = 3$ is illustrated in figure 10.

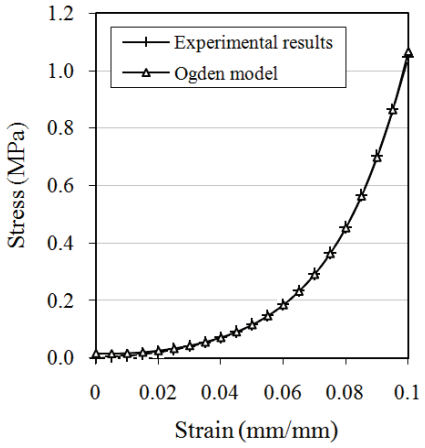


Fig. 10. Average stress–strain behaviour as obtained experimentally for porcine corneas subjected to a strain rate of 25% min$^{-1}$ and the Ogden curve fit result

The results in table 2 show gradual increases in $\mu_1$ and considerably smaller, less consistent increases in $\alpha_1$. Together, these trends indicate that higher strain rates were associated with increases in stress for the same strain, according to equation (3), and increases in tangent modulus for the same stress. Variations in parameters $\mu_2$, $\mu_3$, $\alpha_2$ and $\alpha_3$ were much less influential and only helped improve the fit with the experimental data.

Table 3. Average absolute error per point (in kPa) associated with using Ogden's strain energy function (equation (3)) with $N = 1$, 2 or 3. Percentage values depict the errors of fit compared with the cases with $N = 1$

| Strain rate | Porcine specimens | | | Ovine specimens | | |
|---|---|---|---|---|---|---|
| | $N = 1$ | $N = 2$ | $N = 3$ | $N = 1$ | $N = 2$ | $N = 3$ |
| 0.8% min$^{-1}$ | 0.56 | 0.56 | 0.00 | 22.90 | 1.45 | 0.01 |
| | (100%) | (100.0%) | (0.01%) | (100.0%) | (6.3%) | (0.1%) |
| 8% min$^{-1}$ | 0.37 | 0.37 | 0.00 | 38.50 | 38.26 | 0.59 |
| | (100.0%) | (100.0%) | (0.02%) | (100.0%) | (99.4%) | (1.5%) |
| 25% min$^{-1}$ | 2.82 | 2.82 | 0.01 | 92.18 | 33.06 | 0.34 |
| | (100.0%) | (99.9%) | (0.28%) | (100.0%) | (35.9%) | (0.4%) |
| 42% min$^{-1}$ | 15.91 | 15.89 | 0.11 | 123.94 | 58.83 | 0.63 |
| | (100.0%) | (99.9%) | (0.69%) | (100.0%) | (47.5%) | (0.5%) |
| 83% min$^{-1}$ | 20.95 | 20.91 | 0.14 | 148.40 | 69.25 | 0.80 |
| | (100.0%) | (99.8%) | (0.67%) | (100.0%) | (46.7%) | (0.5%) |
| 210% min$^{-1}$ | 44.61 | 31.38 | 0.14 | 149.23 | 70.91 | 0.74 |
| | (100.0%) | (70.34%) | (0.32%) | (100.0%) | (47.5%) | (0.5%) |
| 420% min$^{-1}$ | 50.02 | 10.32 | 0.08 | 124.48 | 73.51 | 0.54 |
| | (100.0%) | (20.63%) | (0.15%) | (100.0%) | (59.1%) | (0.4%) |

Table 4. Parameters of the anisotropic hyperelastic energy function (equation (4)) that provide the best fit with the experimental results

| Strain rate | Porcine specimens | | | Error/point (MPa) | Ovine specimens | | | Error/point (MPa) |
|---|---|---|---|---|---|---|---|---|
| | $C_{10}$ | $k_1$ | $k_2$ | | $C_{10}$ | $k_1$ | $k_2$ | |
| 0.8% min$^{-1}$ | 0.00464 | 0.90 | 211 | 0.00 | 0.00255 | 9.44 | 283 | 0.03 |
| 8% min$^{-1}$ | 0.00464 | 0.90 | 411 | 0.03 | 0.00255 | 13.89 | 283 | 0.02 |
| 25% min$^{-1}$ | 0.00255 | 4.45 | 211 | 0.04 | 0.00255 | 25.00 | 283 | 0.01 |
| 42% min$^{-1}$ | 0.00255 | 4.45 | 280 | 0.04 | 0.00255 | 25.00 | 750 | 0.03 |
| 83% min$^{-1}$ | 0.00255 | 6.50 | 280 | 0.03 | 0.00255 | 30.00 | 1000 | 0.04 |
| 210% min$^{-1}$ | 0.00255 | 10.00 | 280 | 0.03 | 0.00255 | 40.00 | 1000 | 0.03 |
| 420% min$^{-1}$ | 0.00255 | 10.00 | 322 | 0.03 | 0.00255 | 70.00 | 1000 | 0.01 |

The parameters of the hyperelastic anisotropic function (equation (4)) are finally presented in table 4. The optimisation of the function parameters was based on the assumptions of material incompressibility and two preferred directions (vertical and horizontal) with moderate fibre scatter. The results of the optimisation exercise, which was based on fitting the function to the experimental results, show gradual increases in the values of all parameters with rises in strain rate. Together, these trends indicate higher stresses for the same strain and higher $E$ for the same stress, as has been observed experimentally. The average absolute errors are also included in table 4 and have been found to remain below 0.04 MPa per data point, which was significantly small when considering the stress range of the tests (0–1.2 MPa for porcine corneas and 0–1.35 MPa for ovine corneas).

# 4. Discussion

Determining the sensitivity of the cornea's stress–strain behaviour to strain-rate changes is of great importance for the numerical simulation of corneal response to slow mechanical actions such as intraocular pressure variation with posture change [13] and contact tonometry, and fast actions including eye rubbing [14], [27], sports' and accidental impacts [28] and non-contact tonometry [15]. The strain rates associated with these mechanical actions range widely over several orders of magnitude and may go beyond the range considered in this study (0.8 to 420% per minute). Identifying the effect of strain-rate on the stress–strain response of corneal tissue is essential to ensure that the material constitutive model used in simulation is compatible with the expected strain rate of the mechanical action.

In preparation for work on human corneas, the study started with porcine and ovine tissues because of their wide availability and reasonable similarity in mechanical behaviour and microstructural composition to human corneas [4], [9], [10]. Both porcine and ovine corneas demonstrated strain-rate dependent behaviour with stiffening associated with higher strain rates. This finding is compatible with the known effect of strain rate on collagen fibres, which dominate the cornea's mechanical performance. Similar effect of strain rate on behaviour has been reported before in ocular sclera [29], skin [30]–[32], placenta [33], brain tissue [34], kidney capsular membrane [35] and other biological tissues. The studies further observed increased fracture stresses [36] and decreased fracture strains [35] with higher strain rates.

While in general agreement with earlier findings, the current study revealed considerable differences between porcine and ovine corneas in their response to strain-rate changes. Most notably, while ovine corneas continued to experience increased stiffening (higher tangent modulus) with higher strain rates throughout the full experimental range, porcine corneas' response was significant over only a limited range of low rates. This has been demonstrated, for example, by the small and statistically insignificant increases in tangent modulus of porcine corneas between 25% $min^{-1}$ and 83% $min^{-1}$ and between 83% $min^{-1}$ and 420% $min^{-1}$, which were 4.1 ± 5.7% and 7.2±13.0%, respectively. These were much lower than the corresponding average tangent modulus increases in ovine corneas; 15.5 ± 10.7% and 42.7 ± 15.8%, the latter of which was statistically significant.

A number of theories exist to explain the tissue's sensitivity to strain rate. LANIR believed that much of the sensitivity was attributed to the aligning and uncoiling movement of collagen fibrils in the direction of applied stress [37], while others argued that it was due to decoran proteoglycans and anionic glycosaminoglycan (AGAG) interfibrillar bridges acting as molecular springs in connecting the fibrils together [37]–[39]. However, while available theories may help explain the sensitivity of the tissue to strain rate, they are still unable to reconcile significant differences in behaviour such as those observed in this study between porcine and ovine corneal tissue.

The strip extensometry testing used in this study has a number of well-documented limitations caused by the initially curved form of the specimen and the termination of fibrils along the specimen sides [16], [40]. The straightening of the specimens from their curved form results in initial strains that affect the behaviour under subsequent loading. The relatively large specimen thickness poses a difficulty with the potential of unequal clamping of external and internal tissue layers. The uniaxial loading adopted in strip testing is also different from the biaxial loading expected in intact eye globes, possibly leading to changes in obtained behaviour. Further, since uniaxial testing conditioning is required to establish a recoverable reference state, the repeated loading and unloading are expected to remodel the tissue's micro-structure, aligning collagen fibres more in the direction of load, and affecting the accuracy of the results' representation of real behaviour. Although these limitations affect the technique's suitability to obtain the global properties of corneal tissue, the technique remains viable for comparative studies similar to the present one where the focus is on the variation in tissue behaviour caused by changes in strain rate.

The limitations associated with uniaxial strip testing could be overcome with the use of inflation testing where the tissue is kept intact and loaded with a posterior pressure that closely simulates the intraocular pressure. However, current inflation experimental facilities only allow control of pressure application rates rather than strain rates [1], [7] and would therefore be unsuitable for the current study. This particular limitation has further made it difficult to validate the strain-rate dependent constitutive models presented in this paper.

Validation of the constitutive models is considered essential since the quantification of the models' parameters was based on macroscopic mechanical tests rather than on histological investigations identifying the anisotropy of the tissue's micro-structure. An ideal validation of the constitutive models would be to compare their performance in whole globe numerical models subjected to intraocular pressure elevation against the experimental behaviour of eye globes inflated under strain-controlled conditions. Modifications are currently being introduced to the authors' inflation test rig to enable a strain-controlled loading method, which could be used in future studies to provide relevant inflation behaviour suitable for validating the constitutive models of this study.

## References

[1] ELSHEIKH A., WANG D., BROWN M., RAMA P., CAMPANELLI M., PYE D., *Assessment of corneal biomechanical properties and their variation with age*, Curr. Eye Res., 2007, 32(1), 11–19.

[2] BRYANT M.R., MCDONNELL P.J., *Constitutive laws for biomechanical modeling of refractive surgery*, J. Biomech. Eng., 1996, 118(4), 473–481.

[3] LEONARDI M., LEUENBERGER P., BERTRAND D., BERTSCH A., RENAUD P., *First steps toward noninvasive intraocular pressure monitoring with a sensing contact lens*, Invest. Ophthalmol. Vis. Sci., 2004, 45(9), 3113–3117.

[4] ELSHEIKH A., ALHASSO D., RAMA P., *Biomechanical properties of human and porcine corneas*, Exp. Eye Res., 2008, 86(5), 783–790.

[5] BERTSCH A., LEONARDI M., RENAUD P., *The sensing contact lens*, Med. Device Technol., 2006, 17(5), 19–21.

[6] ELSHEIKH A., WANG D., RAMA P., CAMPANELLI M., GARWAY-HEATH D., *Experimental assessment of human corneal hysteresis*, Curr. Eye Res., 2008, 33(3), 205–213.

[7] BOYCE B.L., GRAZIER J.M., JONES R.E., NGUYEN T.D., *Full-field deformation of bovine cornea under constrained inflation conditions*, Biomaterials, 2008, 29(28), 3896–3904.

[8] ELSHEIKH A., ALHASSO D., *Mechanical anisotropy of porcine cornea and correlation with stromal microstructure*, Exp. Eye Res., 2009, 88(6), 1084–1091.

[9] LEONARDI M., PITCHON E.M., BERTSCH A., RENAUD P., MERMOUD A., *Wireless contact lens sensor for intraocular pressure monitoring: assessment on enucleated pig eyes*, Acta Ophthalmol., 2009, 87(4), 433–437.

[10] HAYES S., BOOTE C., LEWIS J., SHEPPARD J., ABAHUSSIN M., QUANTOCK A.J., PURSLOW C., VOTRUBA M., MEEK K.M., *Comparative study of fibrillar collagen arrangement in the corneas of primates and other mammals*, Anat. Rec. (Hoboken), 2007, 290(12), 1542–1550.

[11] MEEK K.M., LEONARD D.W., *Ultrastructure of the corneal stroma: a comparative study*, Biophys. J., 1993, 64(1), 273–280.

[12] CAREW E.O., BARBER J.E., VESELY I., *Role of preconditioning and recovery time in repeated testing of aortic valve tissues: validation through quasilinear viscoelastic theory*, Ann. Biomed. Eng., 2000, 28(9), 1093–1100.

[13] KOTHE A.C., *The effect of posture on intraocular pressure and pulsatile ocular blood flow in normal and glaucomatous eyes*, Surv. Ophthalmol., 1994, 38, S191–197.

[14] MCMONNIES C.W., BONEHAM G.C., *Experimentally increased intraocular pressure using digital forces*, Eye Contact Lens, 2007, 33(3), 124–129.

[15] LUCE D.A., *Determining in vivo biomechanical properties of the cornea with an ocular response analyzer*, J. Cataract. Refract. Surg., 2005, 31(1), 156–162.

[16] ELSHEIKH A., ANDERSON K., *Comparative study of corneal strip extensometry and inflation tests*, J. R. Soc. Interface, 2005, 2(3), 177–185.

[17] WOO S.L., KOBAYASHI A.S., SCHLEGEL W.A., LAWRENCE C., *Nonlinear material properties of intact cornea and sclera*, Exp. Eye Res., 1972, 14(1), 29–39.

[18] SHAW A.J., COLLINS M.J., DAVIS B.A., CARNEY L.G., *Eyelid pressure and contact with the ocular surface*, Invest. Ophthalmol. Vis. Sci., 2010, 51(4), 1911–1917.

[19] SHAW A.J., DAVIS B.A., COLLINS M.J., CARNEY L.G., *A technique to measure eyelid pressure using piezoresistive sensors*, IEEE Trans. Biomed. Eng., 2009, 56(10), 2512–2517.

[20] SHAW A.J., COLLINS M.J., DAVIS B.A., CARNEY L.G., *Eyelid pressure: inferences from corneal topographic changes*, Cornea, 2009, 28(2), 181–188.

[21] KAMPMEIER J., RADT B., BIRNGRUBER R., BRINKMANN R., *Thermal and biomechanical parameters of porcine cornea*, Cornea, 2000, 19(3), 355–363.

[22] MEEK K.M., BOOTE C., *The use of X-ray scattering techniques to quantify the orientation and distribution of collagen in the corneal stroma*, Prog. Retin. Eye Res., 2009, 28(5), 369–392.

[23] BOYCE B.L., JONES R.E., NGUYEN T.D., GRAZIER J.M., *Stress-controlled viscoelastic tensile response of bovine cornea*, J. Biomech., 2007, 40(11), 2367–2376.

[24] ZENG Y., YANG J., HUANG K., LEE Z., LEE X., *A comparison of biomechanical properties between human and porcine cornea*, J. Biomech., 2001, 34(4), 533–537.

[25] BOOTE C., DENNIS S., HUANG Y., QUANTOCK A.J., MEEK K.M., *Lamellar orientation in human cornea in relation to mechanical properties*, J. Struct. Biol., 2005, 149(1), 1–6.

[26] MEEK K.M., BOOTE C., *The organization of collagen in the corneal stroma*, Exp. Eye Res., 2004, 78(3), 503–512.

[27] MCMONNIES C.W., *Abnormal rubbing and keratectasia*, Eye Contact Lens, 2007, 33(6), 265–271.

[28] UCHIO E., OHNO S., KUDOH J., AOKI K., KISIELEWICZ L.T., *Simulation model of an eyeball based on finite element analysis on a supercomputer*, Br. J. Ophthalmol., 1999, 83(10), 1106–1111.

[29] DOWNS J.C., BURGOYNE C.F., THOMAS K.A., THOMPSON H.W., HART R.T., *Effects of strain rate on the mechanical properties of posterior rabbit sclera*, [in:] Proceedings of the first joint BMES/EMBS Conference Serving Humanity, Advancing Technology, Atlana, GA, USA, 1999.

[30] ZHOU B., XU F., CHEN C.Q., LU T.J., *Strain rate sensitivity of skin tissue under thermomechanical loading*, Philosophical Transactions of the Royal Society A: Mathematical, Physical and Engineering Sciences, 2010, 368(1912), 679–690.

[31] POTTS R.O., CHRISMAN D.A. Jr, BURAS E.M. Jr, *The dynamic mechanical properties of human skin in vivo*, Journal of Biomechanics, 1983, 16(6), 365–372.

[32] DALY C.H., *Biomechanical properties of dermis*, J. Invest. Dermatol., 1982, 79, Suppl 1, 17s–20s.

[33] MANOOGIAN S.J., *Effect of strain rate on the tensile material properties of human placenta*, Journal of Biomechanical Engineering-Transactions of the ASME, 2009, 131(9).

[34] SACK I., BEIERBACH B., WUERFEL J., KLATT D., HAMHABER U., PAPAZOGLOU S., MARTUS P., BRAUN J., *The impact of aging and gender on brain viscoelasticity*, NeuroImage, 2009, 46(3), 652–657.

[35] SNEDEKER J.G., NIEDERER P., SCHMIDLIN F.R., FARSHAD M., DEMETROPOULOS C.K., LEE J.B., YANG K.H., *Strain–rate dependent material properties of the porcine and human kidney capsule*, Journal of Biomechanics, 2005, 38(5), 1011–1021.

[36] SHERGOLD O.A., FLECK N.A., RADFORD D., *The uniaxial stress versus strain response of pig skin and silicone rubber at low and high strain rates*, International Journal of Impact Engineering, 2006, 32(9), 1384–1402.

[37] LANIR Y., *The rheological behaviour of the skin: experimental results and a structural model*, Biorheology, 1979, 16(3), 191–202.

[38] SCOTT J.E., *Elasticity in extracellular matrix "shape modules" of tendon, cartilage, etc. A sliding proteoglycan-filament model*, J. Physiol., 2003, 553(Pt 2), 335–343.

[39] HAVERKAMP R.G., WILLIAMS M.A., SCOTT J.E., *Stretching single molecules of connective tissue glycans to characterize their shape-maintaining elasticity*, Biomacromolecules, 2005, 6(3), 1816–1818.

[40] HOELTZEL D.A., ALTMAN P., BUZARD K., CHOE K., *Strip extensiometry for comparison of the mechanical response of bovine, rabbit, and human corneas*, J. Biomech. Eng., 1992, 114(2), 202–215.